Light-atom diffusion and clustering at crystal surfaces

1997 J. Phys.: Condens. Matter 9 33

(http://iopscience.iop.org/0953-8984/9/1/006)

J. Phys.: Condens. Matter **9** (1997) 33–41. Printed in the UK PII: S0953-8984(97)70953-6

Light-atom diffusion and clustering at crystal surfaces

A A Berzin, A I Morosov and A S Sigov

Moscow State Institute of Radioengineering, Electronics and Automation (Technical University), Prospect Vernadskogo 78, 117454 Moscow, Russia

Received 12 January 1996, in final form 18 September 1996

Abstract. The diffusion of light atoms at a crystal surface is considered. Numerical experiments on diffusion at crystal surfaces of different crystallographic orientation demonstrate the diffusion to be suppressed by the clusterization process. If bound states of two adatoms do not exist at the surface, a quasi-two-dimensional Wigner crystal is formed, resulting thus in a drastic decrease in the diffusion coefficient.

1. Introduction

The theoretical treatment of the diffusion of light atoms adsorbed at a crystal surface (so-called adatoms) revealed that in the case of a repulsive short-range interaction between the adatoms the existence of their bound states is defined by the form of the long-range interaction [1, 2]. The latter in its turn depends heavily on the crystal surface orientation about the crystallographic axes. For some cuts this interaction may be repulsive in nature and no bound states of adatoms arise. For other cuts the interaction may change its sign and this inevitably leads to clustering of adatoms with decreasing temperature, as a result of which a sharp decrease in the diffusion coefficient takes place.

Below the characteristic temperature of clusterization T_c the thermodynamic equilibrium accords with a large-scale exfoliation into quasi-two-dimensional (2D) phases with high and low concentrations of adatoms, but such a thermodynamically equilibrium state is practically unattainable in the event of a slightly covered surface, i.e. for a small value of the ratio x of the numbers of adsorbed atoms and native atoms furnishing the crystal surface. On cooling, the system appears in one of the metastable states characterized by the presence of small clusters of a few adatoms. The initiation of such clusters significantly retards the rate of relaxation to equilibrium, so such a state is not observable on the real time scale.

An analytical description of the diffusion with a number of small clusters of different sizes and shapes presents a considerable challenge. Because of this, we have performed numerical modelling of light-atom diffusion at crystal surfaces.

The results of similar calculations for pure short-range attractive interaction between adatoms, when the cut orientation is not so vital, have already been published [3, 4].

2. Description of the model

The long-range part of the interaction between adatoms at a metal surface is the elastic interaction W_{elas} with added indirect interaction via Friedel oscillations in the electron density W_{el}.

0953-8984/97/010033+09$19.50

The elastic interaction at the (100) cut of a cubic crystal with slight anisotropy has the form

$$W_{elas}(\boldsymbol{\rho}) = \alpha\left[\tfrac{3}{5} - (X/\rho)^4 - (Y/\rho)^4\right]d^3/\rho^3 \tag{1}$$

where d is the interatomic distance, $\boldsymbol{\rho} = (X, Y)$ is the 2D vector parallel to the crystal surface, and the sign of the constant α is given by the sign of the elastic constant combination $2C_{44} + C_{12} - C_{11}$ [5].

In the case of the (111) cut of a cubic crystal one has $W_{elas}(\boldsymbol{\rho}) = \alpha' d^3/\rho^3$, where $\alpha' =$ constant. In the bulk of the crystal one has $\alpha' = 0.1\alpha$, but at the surface the relationship may be different.

To be sure, the form of (1) relates to an infinite and not a semi-infinite crystal. Unfortunately we are not aware of an expression for the Green function for elastic displacements at the crystal surface. Nevertheless, the translational symmetry break in the direction perpendicular to the surface must not break the interaction symmetry at the surface without surface reconstruction. One can consider the isotropic elastic interaction at the (111) cut of a cubic crystal as an example.

The calculations for semi-infinite crystals with weak cubic anisotropy are reduced to derivation of a new, more complicated expression for the quantities α and α' in terms of crystal elastic constants.

The energy of the indirect interaction between adatoms through the Friedel oscillations in the electron density depends strongly upon the Fermi surface shape. Let us begin with the case when the underfilled electron surface band is absent. The fall-off of oscillations in the direction given by a unit vector $\boldsymbol{n} = \boldsymbol{\rho}/\rho$ is derived from an extreme size of the Fermi surface along this direction $2k_F(\boldsymbol{n})$. If the value $k_z = 0$ (k_z is the wavevector component perpendicular to the crystal surface) corresponds to the sole extreme size, then the interaction through the Friedel oscillations in the electron density diminishes as ρ^{-5}:

$$W_{el}(\boldsymbol{\rho}) = W_0 \cos\left[2k_F(\boldsymbol{n})\rho\right]d^5/\rho^5 \qquad W_0 = \text{constant}. \tag{2}$$

This is concerned with a small value of the matrix element of the defecton–electron interaction near a given extreme. This was shown by Law and Kohn [6] for the spherical Fermi surface. If the extreme size of the Fermi surface is related to $k_z = 0$, then one has

$$W_{el}(\boldsymbol{\rho}) = W_0 \cos\left[2k_F(\boldsymbol{n})\rho\right]d^3/\rho^3 \tag{3}$$

as in the bulk [2]. In such a case the Fermi surface is of the form of several pockets or a corrugated cylinder.

For the Fermi surface in the form of a noncorrugated cylinder with the axis perpendicular to the crystal surface the interaction energy is proportional to ρ^{-2} [6].

The Fermi surface is always corrugated in a real crystal. This is why, for small corrugation ($k_F \gg k_F^{max} - k_F^{min}$, k_F^{max} and k_F^{min} being minimum and maximum radii of the corrugated cylinder) an intermediate asymptotic $W_{el}(\boldsymbol{\rho}) \propto \rho^{-2}$ should be observed in the range $(2k_F)^{-1} \ll \rho \ll [2(k_F^{max} - k_F^{min})]^{-1}$, while in the range $\rho \gg [2(k_F^{max} - k_F^{min})]^{-1}$ the interaction energy appears to be proportional to ρ^{-3}.

If there exists a partially occupied surface electron energy band, then the interaction energy falls off as ρ^{-2} [6].

The constants W_0 and α are of the same order of magnitude (10^2–10^3 K) for all cases.

We considered the case of interaction through Friedel oscillations in the electron density described by (3), but if one has $W_{el} \propto \rho^{-5}$ then this term falls off with distance much faster than the elastic interaction, so one can say that the long-range interaction between the adatoms is only caused by the elastic interaction.

Due to the changing sign of both W_{elas} and W_{el} ((1) and (3), respectively) one can conclude that the bound states of adatoms inevitably arise at the (100) cut as the temperature decreases, while their initiation at the (111) cut depends on the sign of the constant α' and on the relationship between α' and W_0. In the case $\alpha' > 0$ and $\alpha' > W_0$, bound states of adatoms must be absent.

When performing the numerical simulation we restricted ourselves to those two cuts. At the (100) cut the equilibrium positions of adsorbed atoms form a square lattice at the crystal surface. We considered a pattern (100×100) of this lattice periodically extended in space, with 100 adatoms within $x = 0.01$. The interaction between the adatoms is described by the couple potential

$$W_{ij} = \left\{ B\left[3/5 - \left(\tilde{x}_{ij}/\tilde{\rho}_{ij}\right)^4 - \left(\tilde{y}_{ij}/\tilde{\rho}_{ij}\right)^4\right] + (1 - B)\,\cos\left(\gamma\tilde{\rho}_{ij}\right)\right\} \Big/ \tilde{\rho}_{ij}^3 \qquad (4)$$

where $\tilde{\rho}_{ij}$ is the radius vector with integer coordinates, which joins two lattice points, and $\gamma = 0.75$ is a coefficient. With such a potential the quantity B defines a relative contribution of the elastic interaction between defects, and the temperature is measured in the units of α/B.

At the (111) cut the equilibrium positions of adatoms form a plane lattice with a rhombic elementary cell whose sides are $2^{1/2}$ times the sides of a square cell at the (100) cut and form an angle of 60°. A pattern of 100×100 elementary cells periodically extended in space was considered with 100 adatoms within. The interaction potential has the form

$$W_{ij} = \left\{0.1B + (1 - B)\,\cos\left(2^{1/2}\gamma\tilde{\rho}_{ij}\right)\right\} \Big/ \left(2^{1/2}\tilde{\rho}_{ij}\right)^3 \qquad (5)$$

where again $\tilde{\rho}_{ij}$ is the dimensionless vector (expressed through the lattice constants) joining the oblique lattice points. With the use of (4) and (5) one can find the adatom potential energy at any lattice point.

To examine the dynamic behaviour of the adatoms we used the Metropolis scheme of the Monte Carlo method [7], with a random sampling of an adatom and a neighbouring lattice point to which this adatom can move. An adatom cannot transfer to an occupied lattice point.

In the case of small concentration of light adatoms their characteristic temperature of clusterization falls within the temperature range where the adatom quantum jump diffusion is essential. Such a jump from an ith occupied point to a neighbouring jth vacant point is accompanied by the change of the given adatom potential energy in the field of all other adatoms

$$\xi_{ij} = \sum_{m \neq i} \left(W_{jm} - W_{im}\right) \qquad (6)$$

where the summation is performed over all particles except the jumping one.

Let J_0 be the tunnelling matrix element for the adatom transition between neighbouring equivalent positions in the absence of disordering, i.e. at $\xi_{ij} = 0$.

Provided the condition $|\xi_{ij}| \gg J_0$ is satisfied, the transition is caused by either interaction with conduction electrons or one-phonon processes. In order of magnitude the probability of the transition followed by the electron scattering is [8]

$$\omega_{el} \sim \left(J_0^2/\overline{h}\xi_{ij}\right) \Big/ \left[\exp\left(\xi_{ij}/T\right) - 1\right] \qquad (7)$$

where $\overline{h}$ is the Planck constant.

The probability of the processes accompanied by phonon irradiation or absorption in order of magnitude approximates to

$$\omega_{ph} \sim \left(J_0^2\tilde{E}\xi_{ij}/\theta^3\overline{h}\right)\left[\exp\left(\xi_{ij}/T\right) - 1\right] \qquad (8)$$

where $\tilde{E}$ is an atomic scale energy and θ is the Debye temperature.

Equations (7) and (8) comprise the full transition probability. The full probability depends slightly on ξ_{ij} at $\xi_{ij} < 0$ and decreases exponentially rapidly at $\xi_{ij} > 0$. This is why the transition probability can be introduced with good accuracy in the form

$$\omega_{ij} = \begin{cases} 1 & \text{if } \xi_{ij} \leqslant 0 \\ \exp\bigl(-\xi_{ij}/T\bigr) & \text{if } \xi_{ij} \geqslant 0. \end{cases} \tag{9}$$

To find the diffusion coefficient we use the Einstein equation

$$D = T\mu \tag{10}$$

where μ is the mobility, i.e. the proportionality coefficient between the directed movement velocity of adatoms and the applied force. By creating a slight potential gradient along one of the crystallographic axes and by adding it to the quantity ξ_{ij}, we realize a random sampling of initial coordinates of the adatoms. After this the system is annealed at a given temperature, i.e. the relaxation to a stationary state takes place. Actually, due to the interaction between adatoms, their reciprocal positions are not random in general. An approach to the stationary regime is monitored by the total potential energy of adatoms.

After reaching the stationary state the flux of particles generated by the applied force is found. The mobility is defined as the ratio of the flux to the force. The magnitude of the force F holds as long as the inequality $Fd \ll T$ is valid. This is necessary because the potential gradient must not change the probability of adatom transition to the neighbouring point.

The choice of temperature dependence of the jump probability in the form given by (9) implies it to be normalized on the basis of probability of the jump of noninteracting adatoms. Therefore the computer simulation results in the ratio D/D_0 (here D_0 is the diffusion coefficient of noninteracting adatoms) and not in the diffusion coefficient D itself.

3. Discussion of results

3.1. Bound states

In figure 1 one can see the temperature dependences of the ratio D/D_0 for the presence of bound states of adatoms at the surface. What all the dependences have in common is that on lowering the temperature a drastic decrease in the magnitude of the ratio D/D_0 comes about, from a value close to unity (at high temperature) to a near-zero value (for the cluster region). It was found in the preceding papers by the present authors [10–12] that

$$D/D_0 = [1 + \beta x \exp(w/T)]^{-1} \tag{11}$$

where $\beta \sim 1$, and w is the characteristic (averaged over the clusters) specific bound energy of adatoms in the cluster. The characteristic temperature of clusterization is

$$T_c = 2/|\ln x|. \tag{12}$$

We approximated the results obtained by the dependence

$$D/D_0 = a[1 + b\exp(c/T)]^{-1} \tag{13}$$

where a, b, and c were free parameters. The parameter a, as we might expect, proved to be equal to unity with an accuracy of several per cent despite $b \sim 10^{-2}$ being calculated with a large error. Shown in table 1 are the values of c and of the clusterization temperature T_c, both found theoretically with the use of (12) and calculated by model experiments for $D/D_0 = 0.5$ for (100) and (111) cuts and for different values of B.

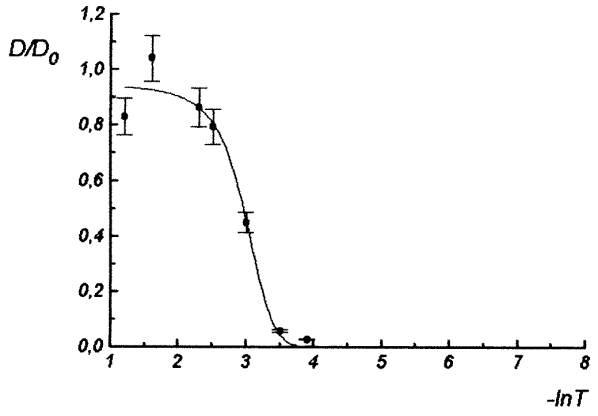

(*a*)

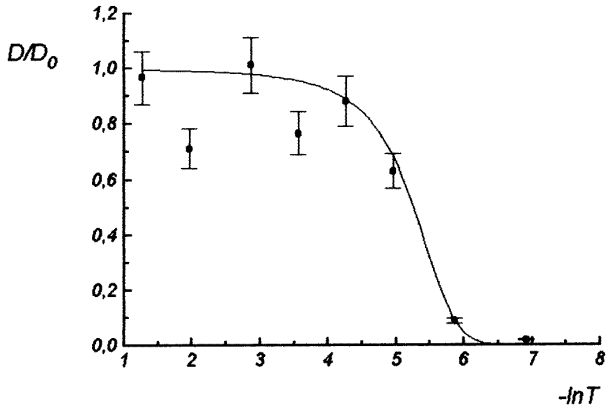

(*b*)

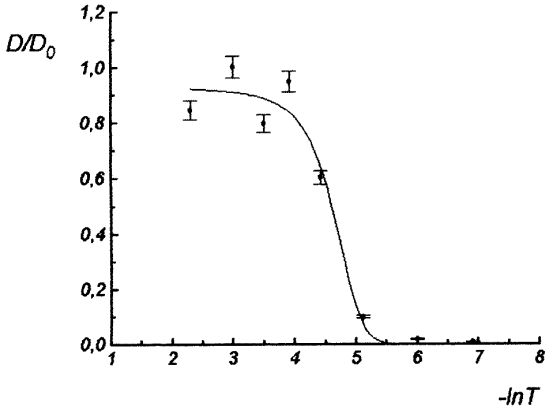

(*c*)

Figure 1. Temperature dependence of the diffusion coefficient of adatoms: (a) for the (100) cut, $B = 0,8$; (b) for the (111) cut, $B = 0.8$; (c) for the (100) cut, $B = 0.5$; (d) for the (111) cut, $B = 0.5$.

Table 1. The values of specific bound energy and clusterization temperature.

N	Cut	B	c	T_c^{calc}	T_c^{exp}
1	(100)	0.8	0.23	0.050	0.051
2	(111)	0.8	0.014	0.0029	0.0051
3	(100)	0.5	0.039	0.0085	0.0097
4	(111)	0.5	0.17	0.036	0.038

The error in quantity D/D_0 displayed in figure 1 is caused by a spread in D/D_0 values at a given temperature and for different initial random distributions of defects, i.e. for different realizations. Such a spread is an outcome of a limitation on the size of the surface pattern under consideration. This result should be taken into account in experimental investigations as well. When scanning tunnelling microscopy is used to seek the adatom diffusion coefficient, a limited part of the surface is scanned; therefore one has to average over different parts of the surface or differential initial distributions of the adatoms.

The diminution of the ratio D/D_0 is due to the clustering of defects and this is demonstrated by figure 2, where the distribution of adatoms at the crystal surface for $T > T_c$ and $T < T_c$ is shown. At $T \gg T_c$, the correlations in the positions of adatoms are very small, if any (figure 2(a)). At $T \ll T_c$, small clusters arise, their shape and size being defined by the interaction (the value of B) and by the crystal surface cut orientation (figure 2(b)–(e)). A change in the constant B magnitude may be variously manifested at different cuts. If $B = 0.5$, the nearest neighbours in the cluster are located at intervals of one lattice point for both (100) and (111) cuts (figure 2(b) and (d)). With increasing magnitude of B up to $B = 0.8$, the adatoms are at nearest points at the (100) cut (figure 2(c)), whereas the cluster structure appears to be looser at the (111) cut (figure 2(e)). This is due to anisotropy and the oscillating nature of the interaction as well as to a difference in parameters of the lattice formed by equilibrium positions of the adatoms at different crystal cuts.

It should be noted that the occurrence of chainlike clusters in [010] and [001] directions at the (100) cut is caused by the anisotropy of the elastic interaction between adatoms. Somewhat similar chains of indium atoms arose at the (100) cut of Cu in first-principles numerical calculations within the framework of the microscopic model [13].

Owing to a low specific bound energy small clusters become unstable and one can see the formation of one large cluster (figure 2(f)).

The results of numerical calculations shown in figure 2 allow one to see that the number of free (non-clusterized) adatoms is small at $T \ll T_c$. Equation (11) has been derived under the assumption that the main contribution to the diffusion is due to non-clusterized particles whose concentration is exponentially small at $T \ll T_c$. What actually happens is that the cluster mobility is a non-zero quantity, which depends on the cluster shape and number of particles within and is of an activating nature [14, 15]. In the modelling performed both contributions were taken into account.

Indeed, processes in which one of the adatoms does not break free from its cluster but moves along the cluster periphery in the diffusion direction are allowed. After this, another atom of this cluster does the same, etc. As a result, the whole cluster can transfer to another crystal region in the absence of adatom ‘evaporation’ and ‘condensation’ processes.

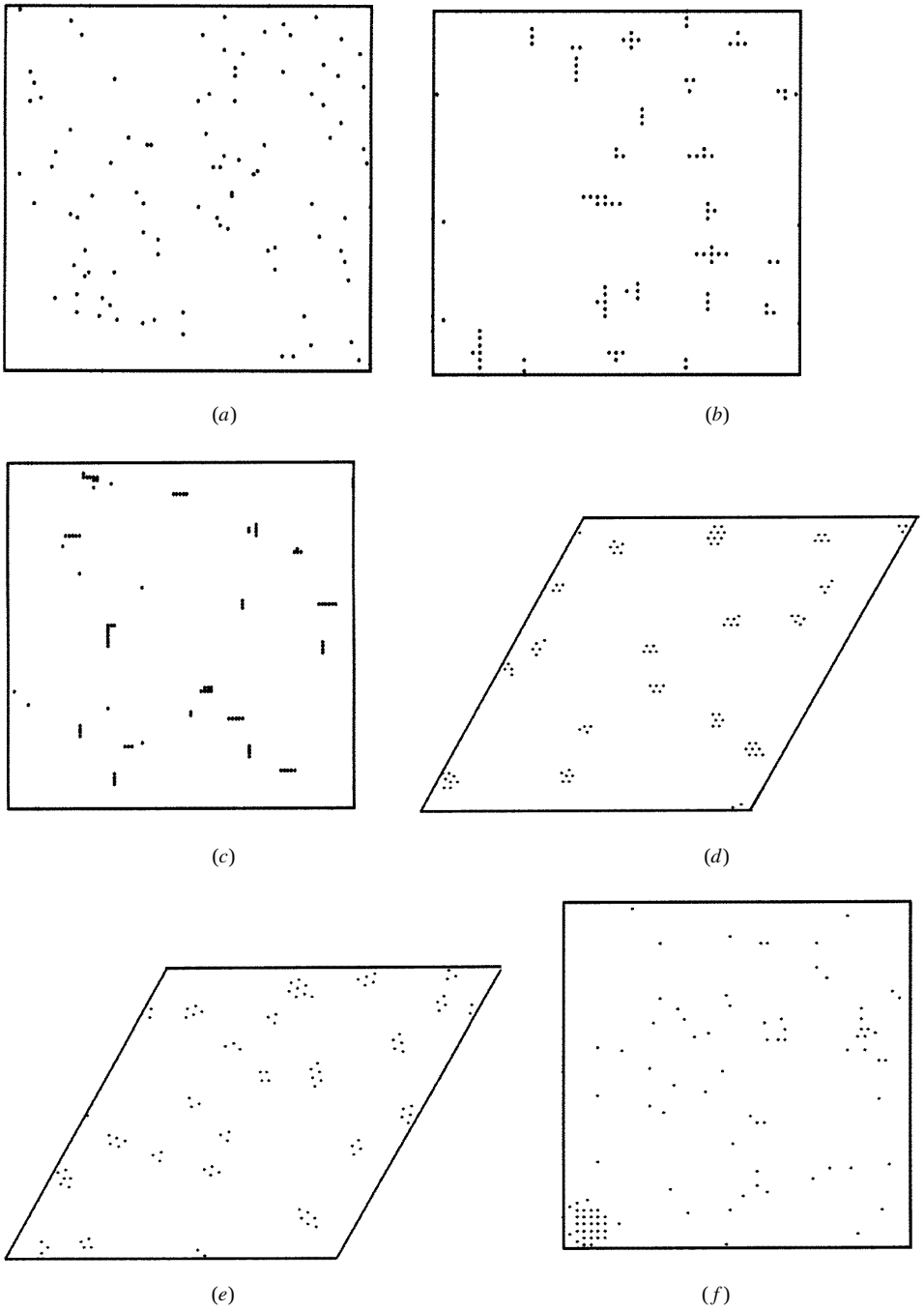

Figure 2. The distribution of adatoms at the crystal surface: (a) for the (100) cut, $B = 0.8$, $T = 0.3$; (b) for the (100) cut, $B = 0.5$, $T = 0.001$; (c) for the (100) cut, $B = 0.8$, $T = 0.03$; (d) for the (111) cut, $B = 0.5$, $T = 0.005$; (e) for the (111) cut, $B = 0.8$, $T = 0.001$; (f) for the (100) cut, $B = 0.5$, $T = 0.012$.

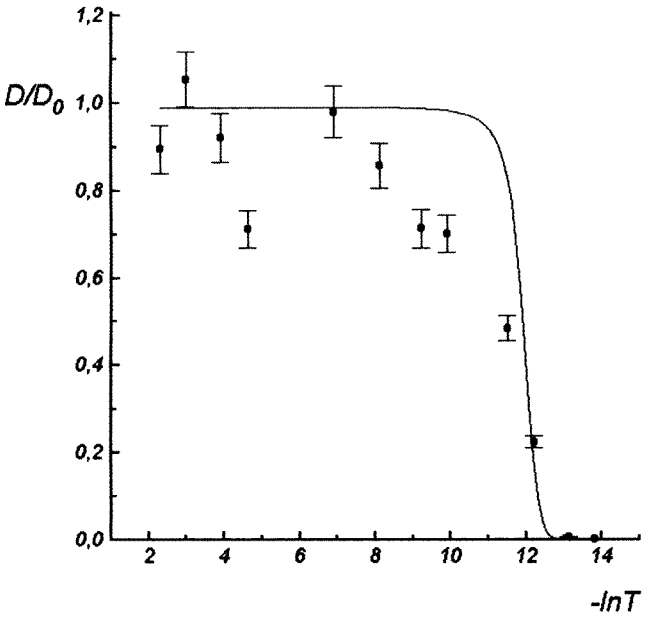

Figure 3. Temperature dependence of the adatom diffusion coefficient in the absence of bound states for the (111) cut, $B = 1$.

3.2. The Wigner crystal

The case $B = 1$ for the (111) cut, when bound states of adatoms do not occur because of the pure repulsive nature of the interaction between adatoms, is considered separately. The pure repulsive interaction affects the diffusion at significantly lower temperature than in the case of the presence of bound states.

Let us estimate the characteristic temperature below which the 2D Wigner crystal of adatoms is formed. Since the elastic interaction between adatoms falls off with distance as ρ^{-3} (1), its energy at mean distances $\langle\rho\rangle \sim x^{-1/2}d$ comprises $T^* \simeq 0.1(x/2)^{3/2}B$, i.e. it may be estimated as 4.4×10^{-5} for $B = 1$ and $x = 2 \times 10^{-2}/3^{1/2}$. A stronger concentration dependence of the quantity T^* in comparison with that of T_c should be noted. The temperature dependence of the diffusion coefficient in this instance is shown in figure 3. By the use of its approximation in the form given by (13) one finds $c = 2.2 \times 10^{-5}$.

It is just at the temperature $T \sim 10^{-5}$ that the value of D/D_0 begins to depart from unity, and at $T \ll T^*$, a plane triangular lattice of adatoms is formed, similar to the lattice of Abrikosov filaments at a superconductor surface. A view of such a 2D Wigner crystal is shown in figure 4. The crystal formation gives rise to adatom localization and to exponential decrease in the quantity D/D_0.

4. Conclusions

(i) The potential energy of the interaction of defects at the metal surface through the Friedel oscillations in the electron density falls off with a distance between defects as ρ^{-p} (the exponent p being equal to 2, 3, or 5 depending on the Fermi surface shape).

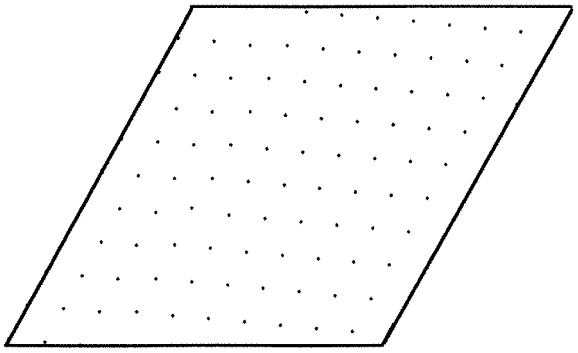

Figure 4. The 2D Wigner crystal of adatoms.

(ii) If bound states of defects exist, the clusterization of defects takes place, resulting in drastic changes in diffusivity.

(iii) The shape of the clusters arising at the surface essentially depends on the surface orientation with respect to crystallographic axes, which is governed by the nature of anisotropy of the long-range interaction between adatoms.

(iv) If bound states of adatoms at the crystal surface are absent the 2D Wigner crystal is formed in the range of low temperatures, resulting in an essential decrease in surface diffusivity as well.

Acknowledgment

This work is partially supported by the grant N94-7.10-3091 of the Russian Federation State Committee for Higher Education.

References

[1] Morosov A I and Sigov A S 1994 *Surf. Sci.* **307–309** 614
[2] Morosov A I and Sigov A S 1995 *Fiz. Tverd. Tela* **37** 691 (Engl. transl. 1995 *Sov. Phys.–Solid State* **37**)
[3] Ala-Nissila T, Kjoll J and Ying S C 1992 *Phys. Rev.* B **46** 846
[4] Cao P-L 1994 *Phys. Rev. Lett.* **73** 2595
[5] Masumyra R A and Scines G 1970 *J. Appl. Phys.* **41** 3930
[6] Law K H and Kohn W 1978 *Surf. Sci.* **75** 69
[7] Binder K (ed) 1979 *Monte Carlo Methods in Statistical Physics* (Berlin: Springer)
[8] Kagan Yu and Prokof'ev N V 1986 *Zh. Eksp. Teor. Fiz.* **90** 2176 (Engl. transl. 1986 *Sov. Phys.–JETP* **63** 1267)
[9] Jackle J, Piche L, Arnold W and Hunklinger S 1976 *J. Non-Cryst. Solids* **20** 365
[10] Morosov A I and Sigov A S 1988 *Solid State Commun.* **67** 841
[11] Morosov A I and Sigov A S 1989 *Zh. Eksp. Teor. Fiz.* **95** 170 (Engl. transl. 1989 *Sov. Phys.–JETP* **68** 97)
[12] Morosov A I and Sigov A S 1994 *Usp. Fiz. Nauk* **164** 243 (Engl. transl. 1994 *Sov. Phys.–Uspekhi* **37** 229)
[13] Breeman M, Barkema G T and Boema D O 1994 *Phys. Rev.* B **49** 43 871
[14] Kellogg G L 1994 *Phys. Rev. Lett.* **73** 1833
[15] Wen J M, Chang S-L, Burnett J W, Evans J W and Thiel P A 1994 *Phys. Rev. Lett.* **73** 2591